Viscous liquid films on a porous vertical cylinder : dynamics and stability

Ding, Zijing; Wong, Teck Neng; Liu, Rong; Liu, Qiusheng

2013

Ding, Z., Wong, T. N., Liu, R., & Liu, Q. (2013). Viscous liquid films on a porous vertical cylinder: Dynamics and stability. Physics of Fluids, 25(6), 064101.

https://hdl.handle.net/10356/101534

https://doi.org/10.1063/1.4808112

Viscous liquid films on a porous vertical cylinder: Dynamics and stability

Zijing Ding, Teck Neng Wong, Rong Liu, and Qiusheng Liu

Citation: Physics of Fluids (1994-present) **25**, 064101 (2013); doi: 10.1063/1.4808112
View online: http://dx.doi.org/10.1063/1.4808112
View Table of Contents: http://scitation.aip.org/content/aip/journal/pof2/25/6?ver=pdfcov
Published by the AIP Publishing

PHYSICS OF FLUIDS **25**, 064101 (2013)

Viscous liquid films on a porous vertical cylinder: Dynamics and stability

Zijing Ding,[1] Teck Neng Wong,[1,a)] Rong Liu,[2] and Qiusheng Liu[2,b)]
[1]*School of Mechanical and Aerospace Engineering, Nanyang Technological University, Singapore 639798*
[2]*Key Laboratory of Microgravity (National Microgravity Laboratory), Institute of Mechanics, Chinese Academy of Sciences, Beijing 100190, China*

(Received 24 October 2012; accepted 15 May 2013; published online 6 June 2013)

In this paper, liquid films flowing down a porous vertical cylinder were investigated by an integral boundary layer model. Linear stability and nonlinear evolution were studied. Linear stability results of the integral boundary layer model were in good agreement with the linearized Navier-Stokes equations which indicated that the permeability of the porous medium enhanced the instability of the flow system. The growth rate and cut-off wave number increased with increasing the permeability and the Reynolds number. Linear stability analysis showed that the system was more unstable for a larger Reynolds number Re. Nonlinear studies showed that, for a very small Re, the film evolved with time while a saturated state was not observed. In addition, it was observed that the film ruptured when the permeability parameter $\beta > 0$, and the rupture time decreased with increasing β. However, for a moderate Reynolds number, a small finite harmonic disturbance evolved to a saturated traveling wave. Further investigation was conducted on the droplet-like wave solution. Results showed that the wave speed increased as the permeability parameter increased. © *2013 AIP Publishing LLC*. [http://dx.doi.org/10.1063/1.4808112]

I. INTRODUCTION

The flow of a thin liquid film down a vertical cylinder subject to the gravity is of great importance for industrial applications. Numerous studies have been carried out on falling films after the experimental work of Kapitza and Kapitza[1] who conducted research on a liquid film falling down an inclined plate. However, in the past decades, many experiments on thin liquid films flowing down vertical cylinders were conducted due to the simplification in measurements.[2–4]

The azimuthal curvature distinguishes the core-annular flow system from the planar flow system. The surface tension plays a stabilizing factor in the planar plane configuration, while it is a destabilizing factor in the core-annular flow system. Lord Rayleigh[5] first explained the physical mechanism of droplet's formation in a liquid jet under the action of the surface tension. A detailed review of free film breakup and droplet formation literature was provided by Eggers.[6]

Theoretical studies on the flow of thin films down the outer surface of a vertical cylinder were first carried out by Goren.[7] Goren[7] analyzed the linear stability of a liquid thread at rest, and investigated the influences of surface tension and the ratio between liquid thickness and radius of the solid substrate. Lin and Liu[8] performed linear stability analysis on a thin falling film flowing down the outside or inside of a vertical tube. Their results showed that the flow system was unstable under the influence of surface tension.

Experimental observations of finite-amplitude interfacial waves in core-annular flow system were conducted by Quéré[2] and De Ryck and Quéré.[9] Successively, Frenkel[10] derived an asymptotic

a)Author to whom correspondence should be addressed. Electronic mail: mtnwong@ntu.edu.sg
b)liu@imech.ac.cn

model equation to study the problem of a very large radius cylinder coated with very thin liquid films. Kliakhandler *et al.*[11] analyzed creeping flow (the Reynolds number $Re = O(1)$) on a vertical fiber and proposed a Benney-type model. Unlike Frenkel's[10] work, the model developed by Kliakhandler *et al.*[11] considered relatively thick liquid films and examined the linear stability of the flow system. Linear stability results by Kliakhandler *et al.*[11] agreed with results by the linearized Navier-Stokes equations when Re was very small, i.e., $Re \approx 0$. In addition, the nonlinear evolution investigation of the interfacial shape subjected to a small finite-amplitude disturbance was also carried out. Hereafter, we denote the model by Kliakhandler *et al.*[11] as *KDB* model for simplicity.

Since saturated traveling waves were observed in thin liquid film flow systems,[2,9] many researchers investigated the non-deformation waves. Pumir *et al.*[12] discussed solitary waves in a falling film down an inclined planar substrate by the Benney equation. Trifonov[13] studied steady-state traveling waves in the viscous flow down vertical wires and derived a two-equation model. Craster and Matar[14] extended the study of Kliakhandler *et al.*[11] and investigated the droplet-like phenomenon theoretically and experimentally. The problem of thin liquid films flowing down a vertical fiber at moderate flow rates was extended by Sisoev *et al.*[15] A two-equation model based on the boundary layer equations was proposed. Linear stability analysis showed that the two-equation model[15] was more accurate than Benney-type equation[11] for a moderate Re. The bifurcation theory was employed by Sisoev *et al.*[15] to study traveling waves in the flow system. Furthermore, the phenomenon of solitary waves in core-annular flow system was investigated by Shkadov *et al.*[16] through the two-equation model.

A more accurate two-equation model based on weighted-residual theory was proposed by Ruyer-Quil and Manneville to study thin liquid films flowing down inclined planes[17,18] and vertical cylinders.[19] Their model is essential for high Re flow and can overcome the nonphysical blow-up phenomenon. Recently, Ruyer-Quil and Kalliadasis[20] extended this two-equation model to study nonlinear waves in the viscous film flowing down a vertical fiber. It was observed that the weighted-residual model[20] was very complex.

In industry and biological systems, the porous fiber has wide applications, such as in prosthetic devices for replacement and reconstruction of bone structure in the skeletal system of humans or animals and filtration systems in market. When considering a liquid film flowing down a vertical porous cylinder or fiber, the permeability of the liquid-porous interface makes it more complex than that on a solid impermeable cylinder. To describe the boundary conditions at the liquid-porous interface, Beavers and Joseph[21] proposed an empirical formula. A one-sided model based on neglecting the dynamics of liquids in the porous medium was carried out by Pascal[22] to examine the influences of permeability on the stability of a thin liquid film falling down an inclined porous plate. Results by Pascal showed that the permeability of porous substrate enhanced the instability of flow system. Pascal further extended this model[22] to a non-Newtonian liquid film.[23]

Sadiq and Usha[24] derived a Benney-type equation to investigate a Newtonian liquid film flowing down an inclined porous plate. The weakly nonlinear analysis was applied to study the supercritical and subcritical stabilities of the flow system. Nonlinear evolution studies showed that, in the supercritical stable region, small finite-amplitude disturbances evolved to permanent finite-amplitude waves. An interesting phenomenon observed was that amplitudes of these permanent waves were either time-independent or time-dependent, and the oscillation behavior in the heights of the time-dependent permanent waves was promoted by the porous substrate. Extension work of a conducting liquid film flowing down an inclined porous plate in the presence of electric field was investigated by Uma and Usha.[25] Recently, Samanta *et al.*[26] considered a liquid film flowing down a slippery inclined plate and derived a weighted-residual model to investigate high Reynolds number flow. Their results showed that the phase speed of the first kind solitary wave was promoted by the slippery boundary. Instead of using the one-sided model, Liu and Liu[27] proposed a two-sided model to investigate the stability of a falling film on a porous substrate. Results of the two-sided model revealed that filtration at the liquid-porous interface played an important role in determining the unstable mode when the Reynolds number was large. Liu and Liu[28] further examined the non-modal instability of the flow system by the one-sided model.

Recently, Ding and Liu[29] investigated a thin liquid film falling down a porous vertical cylinder. They derived a Benney-type model to investigate the stability of the flow system. Their results

showed that the instability of the system was enhanced by the permeability of the porous cylinder. It was observed that the model by Ding and Liu[29] can only describe very small Reynolds number flow. Furthermore, we observed that (i) their model showed that growth rate of disturbances was independent of the Reynolds number, which did not agree with the results of linearized Navier-Stokes equations even when $Re = 1$; (ii) the cut-off wave number by the Benney-type model[29] was independent of Re as well as the permeability parameter, which did not agree with the linearized Navier-Stokes equations; (iii) the linear wave speed by the Benney-type model[29] was independent of wavenumber, contrary to the results of linearized Navier-Stokes equations; (iv) the Benney-type model failed to describe strong nonlinear phenomenon because it neglected the inertia term in the streamwise momentum equation.

In this paper, we derive a two-equation model based on the boundary layer equations to investigate the dynamics of an annular liquid film falling down a vertical porous cylinder. The inertia term is taken into account in the two-equation model which was neglected in Ref. 29. The structure of this paper is organized as follows. The mathematical formulation is constructed in Sec. II. In Sec. III, the integral boundary layer (*IBL*) model is derived to study the linear stability and nonlinear time-dependent evolution of flow system. Further discussion on droplet-like wave solution is carried out in Sec. IV. The results are summarized in Sec. V.

II. MATHEMATICAL FORMULATION

Consider a two dimensional layer of liquid film flowing down a porous vertical cylinder under the influence of gravity as shown in Figure 1. The liquid is Newtonian with constant density ρ, kinematic viscosity ν, and dynamical viscosity $\mu = \rho\nu$. The surface tension σ is assumed to be constant. It is assumed that the flow through the porous medium is governed by Darcy's law. The

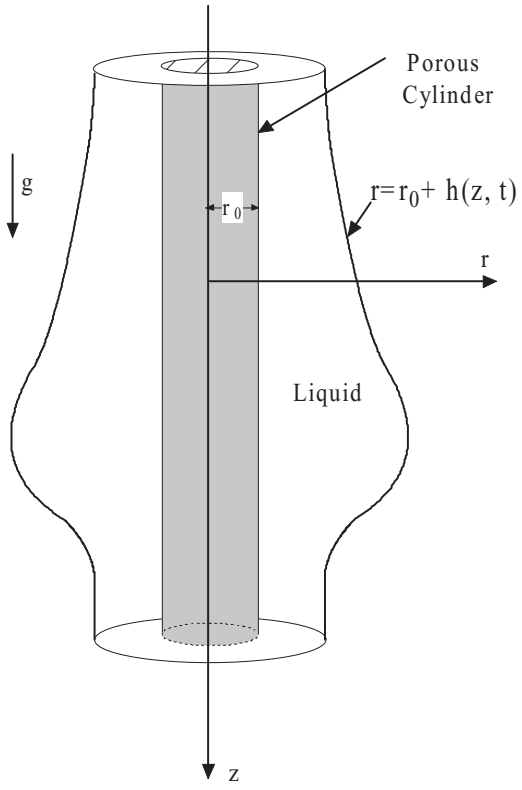

FIG. 1. The geometry of the film flow down a porous vertical cylinder.

experimental investigation by Beavers and Joseph[21] established the condition for tangential velocity at the liquid-porous interface. Considering liquids flowing on a porous cylinder, the condition[21] for the tangential velocity is specialized as

$$\mathbf{n} \cdot \nabla w^* = \frac{\hat{\alpha}}{\sqrt{K}}(w^* - w_p^*), \tag{1}$$

in which w^*, w_p^* are dimensional velocities parallel to the axis (hereafter, the superscript * represents the dimensional variable), and each represents velocity in the liquid film and in the porous medium, respectively (hereafter, the subscript p represent the porous medium). $\hat{\alpha}$ is a dimensionless parameter dependent on the micro-structure of porous medium, and K is the permeability of porous medium. $\mathbf{n}$ is the liquid-porous surface normal and ∇ is the gradient operator.

Velocity in the radial direction is assumed not to vary across the boundary layer formed at the top of the porous medium. At the liquid-porous interface,

$$u^* = u_p^*, \tag{2}$$

where u^*, u_p^* are velocities in the radius direction.

According to the Darcy's Law, fluid in the porous medium is governed by

$$r^{*-1}(r^* u_p^*)_{r^*} + w_{p,z^*}^* = 0, \tag{3}$$

$$w_p^* = -\frac{K}{\mu}(p_{p,z}^* - \rho g), \tag{4}$$

$$p_{p,r^*}^* = 0. \tag{5}$$

The subscripts r^*, z^*, represent derivatives with respect to r^*, z^*, respectively. Pressure is assumed to be constant across the boundary layer; and it is assumed that $p_p^* = p^*$ at the liquid-porous interface. Solving the governing equations together with the pressure condition at the liquid-porous interface, we obtain

$$w_p^* = -\frac{K}{\mu}(p_z^* - \rho g). \tag{6}$$

If W_0 denotes the axial velocity scale, while L (which is proportional to a typical wave length) and h_0 (the mean thickness of the liquid film) denote the axial and radial length scales, respectively, in the liquid film layer, then the pressure scale is

$$P \sim \frac{\mu W_0 L}{h_0^2}, \tag{7}$$

and velocity scale in the porous medium is

$$W_p \sim \frac{K W_0}{h_0^2}. \tag{8}$$

If the pore space geometry is such that the flow is much slower than that of the liquid film, $\frac{K}{h_0^2} \ll 1$, then the mean filter velocities are negligible, so that Eqs. (1) and (2) reduce to

$$\beta_s \mathbf{n} \cdot \nabla w^* = w^*, \tag{9}$$

$$u^* = 0. \tag{10}$$

The parameter $\beta_s = \frac{\sqrt{K}}{\hat{\alpha}}$. The reduced boundary condition Eq. (9) is similar to the Navier slip boundary condition $w^* = l_s \mathbf{n} \cdot \nabla w^*$. Here, l_s is the effective slip length, which can be related to the permeability K and the empirical dimensionless parameter $\hat{\alpha}$ of Beavers and Joseph's[21] boundary condition by $l_s = \beta_s$.

TABLE I. Typical values of α and permeability K.

$\hat{\alpha}$	0.78	1.45	4.0
K (m^2)	9.68×10^{-9}	3.94×10^{-8}	8.19×10^{-8}

Introducing the length scale h_0, the time scale h_0^2/ν, the velocity scale ν/h_0, and the pressure scale $\rho\nu^2/h_0^2$, the system is governed by the dimensionless continuity equation and momentum equations

$$r^{-1}(ru)_r + w_z = 0, \tag{11}$$

$$\frac{Du}{Dt} = -p_r + \nabla^2 u - \frac{u}{r^2}, \tag{12}$$

$$\frac{Dw}{Dt} = -p_z + \nabla^2 w + Re, \tag{13}$$

where $\frac{D}{Dt} = \partial_t + u\partial_r + w\partial_z$ is the material derivative operator. For a prescribed $Re = \frac{gh_0^3}{\nu^2}$, one can change the value of g in the micro-gravity environment.

At $r = r_0$, dimensionless boundary conditions are

$$\beta w_r = (1 - \frac{\beta}{r_0})w, \quad u = 0, \tag{14}$$

where $\beta = \beta_s/h_0$, and $r_0 = r_0^*/h_0$ is the dimensionless radius.

According to the work of Beavers and Joseph,[21] the typical values of $\hat{\alpha}$ and K of the foam metal are listed in Table I. In this paper, we consider a much wider range of permeability K. For instance, for clean sand, in terms of unit m^2, the permeability K is from a range of 10^{-12} to 10^{-9}. Pascal[22] proposed that the dimensionless slip length $\beta = \beta_s/h_0$ ranges from 0 to 0.3. We follow the work of Pascal[22] and suggest that β can have a range of 0–0.4 as proposed by Ding and Liu.[29] Liquids are considered to be composed of silicon oil, and the gravity acceleration can be changed in micro-gravity environment. The range of values for parameters is listed in Table II. The radius of porous cylinder is assumed to be much larger than the mean thickness of liquid film, and the dimensionless radius $r_0 \geq 5$. Therefore, $\beta/r_0 \ll 1$, hence, boundary conditions at the liquid-porous interface can be approximately written as

$$\beta w_r = w, \quad u = 0. \tag{15}$$

At free surface $r = r_0 + h(z, t)$, the non-dimensional stress balance conditions are

$$-p - \frac{2[(w_r + u_z)h_z - u_r - w_z h_z^2]}{1 + h_z^2} = 2HS, \tag{16}$$

$$\frac{(u_z + w_r)(1 - h_z^2) + 2h_z(u_r - w_z)}{1 + h_z^2} = 0. \tag{17}$$

The dimensionless mean curvature $2H = \frac{1}{r_1} + \frac{1}{r_2}$, where $\frac{1}{r_1} = -\frac{1}{(h+r_0)(1+h_z^2)^{1/2}}$ and $\frac{1}{r_2} = \frac{h_{zz}}{(1+h_z^2)^{3/2}}$ are the two principal curvatures of the free surface. The non-dimensional surface tension $S = \frac{\sigma h_0}{\rho\nu^2}$.

TABLE II. Typical values of this system.

Thickness (h_0)	Kinematic viscosity (ν)	Gravity (g)	Reynolds number (Re)
$[10^{-4}, 10^{-3}]$ (m)	$[10^{-6}, 10^{-5}]$ (m^2/s)	$[10^{-1}, 10]$ (m/s^2)	$[10^{-1}, 10]$

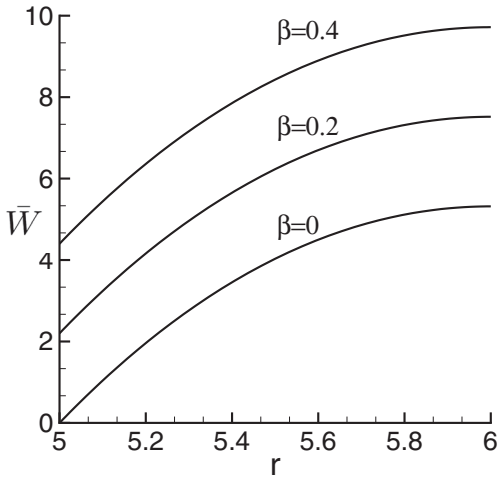

FIG. 2. The profiles of the base velocities for $Re = 10$ and $r_0 = 5$.

The dimensionless kinematic condition of the free surface $r = r_0 + h(z, t)$ is written in the conservative form

$$h_t + (h + r_0)^{-1}\left(\int_{r_0}^{h+r_0} wr\,dr\right)_z = 0. \tag{18}$$

The flow rate q is defined by $\int_{r_0}^{r_0+h} r\,w\,dr$.

The base state of velocity profile is parallel to the cylinder axis such that velocity in the radial direction vanishes. The velocity in the axial direction obtained is as follows:[29]

$$\bar{W} = \frac{-Re}{4}[(r^2 - r_0^2) - 2(r_0 + 1)^2 \ln\frac{r}{r_0}] - \frac{Re\beta}{2}[r_0 - \frac{(r_0 + 1)^2}{r_0}]. \tag{19}$$

Pressure p of base state is constant. Figure 2 shows the velocity profile of base state. In previous studies, it was well-known that the profile of base velocity greatly affects the stability of flow system, such as Rayleigh's inflection point criterion and Fjortoft's criterion. Thus, it is necessary to study the stability of the flow system. A normal mode analysis is achieved by decomposing x into $x = \bar{X} + X\exp(ikz + \lambda t)$, where $\bar{X}$ refers to the base state, and X is the infinitesimal amplitude of a harmonic disturbance with wave number k and complex temporal growth rate λ.

Linearization of the governing equations (11)–(13) leads to the eigenvalue problem,

$$r^{-1}(rU)_r + ikW = 0, \tag{20}$$

$$\lambda U = -P_r + \mathscr{L}U - \frac{U}{r^2} - ik\bar{W}U, \tag{21}$$

$$\lambda W = -ikP + \mathscr{L}W - (ik\bar{W}W + \bar{W}_r U), \tag{22}$$

where the operator $\mathscr{L} = \frac{\partial^2}{\partial r^2} + \frac{1}{r}\frac{\partial}{\partial r} - k^2$.

At $r = r_0$, boundary conditions for the eigenvalue problem are

$$\beta W_r = W, \tag{23}$$

$$U = 0. \tag{24}$$

At $r = 1 + r_0$, the linearized boundary conditions for the eigenvalue problem are

$$P - 2U_r + [2ik\bar{W}_r + S(-k^2 + \frac{1}{(r_0+1)^2})]\eta = 0, \tag{25}$$

$$ikU + W_r + \bar{W}_{rr}\eta = 0, \tag{26}$$

$$\lambda\eta + ik\bar{W}\eta = U, \tag{27}$$

where η measures the deformation of the free surface, which is much smaller than unit.

To resolve the eigenvalue problem, the Chebyshev collocation method is implemented, and the results of the above linearized Navier-Stokes equations will be shown in Sec. III. In this paper, 20 terms of the Chebyshev polynomials are sufficient to provide adequate resolution with economic consumption of computational cost.

III. INTEGRAL BOUNDARY LAYER MODEL

In this section, we derive the nonlinear evolution equations governing the thickness of the film h and the flow rate q based on the Prandtl boundary layer equations.[16] It is assumed that the velocity in the radius direction u is much smaller than the axial component w. Furthermore, the inertia and the viscous terms in Eq. (12) as well as the viscous term w_{zz} in Eq. (13) are assumed to be of higher order and can be neglected. Hence, fluids in the liquid layer can be governed by the dimensionless Prandtl boundary layer equations:[16]

$$\frac{Dw}{Dt} = -p_z + \frac{1}{r}\partial_r(r\partial_r w) + Re, \tag{28}$$

$$p_r = 0, \tag{29}$$

where velocity in the radius direction can be obtained from the continuity equation (11). In the tangential stress balance condition (17), terms of order ∂_z are neglected,

$$w_r|_{r=r_0+h} = 0. \tag{30}$$

The interfacial curvature is approximately written as

$$2H = h_{zz} - \frac{1}{h + r_0}. \tag{31}$$

The term h_{zz} is retained, which is motivated by large amplitude of waves, and the relatively large interface gradients (Klikhandler *et al.*[11] and Craster and Matar[14]). Equation (31) was proposed by Lister *et al.*[31] As the pressure dominates the viscous stress in Eq. (16), the normal stress balance condition reduces to

$$p = -S(h_{zz} - \frac{1}{h + r_0}). \tag{32}$$

Boundary conditions at $r = r_0$ and the kinematic condition of the free surface $r = r_0 + h(z, t)$ are the same as Eqs. (15) and (18), respectively.

To derive the evolution equations, the so-called von-Karman-Pohlhausen technique is applied. Furthermore, the evolution equations for the film thickness h and flow rate q are derived by assuming that the axial velocity w has the following profile:

$$w = \frac{q}{\phi(h)}[(r_0 + h)^2 \ln\frac{r}{r_0} - \frac{1}{2}(r^2 - r_0^2) - \beta(r_0 - \frac{(r_0 + h)^2}{r_0})], \tag{33}$$

in which

$$\phi(h) = \frac{(r_0 + h)^4}{2}\ln\frac{r_0 + h}{r_0} - \frac{[(r_0 + h)^2 - r_0^2][3(r_0 + h)^2 - r_0^2]}{8} + \frac{\beta h^2(h + 2r_0)^2}{2r_0}. \tag{34}$$

Equation (33) satisfies the boundary conditions Eqs. (15) and (30). Multiplying Eq. (28) by r on both sides, and integrating it between r_0 and $r_0 + h$, we obtain

$$\frac{\partial q}{\partial t} + \frac{\partial \mathscr{M}}{\partial z} = \frac{h(2r_0+h)}{2}[S(h_{zz} - \frac{1}{h+r_0})_z + Re - \frac{2q}{\phi(h)}], \tag{35}$$

where $\mathscr{M} = \int_{r_0}^{r_0+h} r w^2 dr = \frac{q^2}{\phi^2}\mathcal{F}(h)$ and

$$\begin{aligned}\mathcal{F}(h) = {} & \frac{(r_0+h)^6}{2}\ln^2\frac{r_0+h}{r_0} - \frac{(r_0+h)^4}{4}[(r_0+h)^2 + 2h(2r_0+h)(1-\frac{2\beta}{r_0})]\ln\frac{r_0+h}{r_0} \\ & + \frac{h^3(2r_0+h)^3}{2r_0^2}\beta^2 - \frac{h^2(2r_0+h)^2[2(r_0+h)^2 + h(2r_0+h)]}{4r_0}\beta \\ & + \frac{h(2r_0+h)[6(r_0+h)^4 + h(2r_0+h)(9r_0^2 + 22r_0h + 11h^2)]}{48}.\end{aligned}$$

The kinematic condition (18) leads to another equation for h and q:

$$\frac{\partial h}{\partial t} + \frac{1}{h+r_0}\frac{\partial q}{\partial z} = 0. \tag{36}$$

The evolution equations (35) and (36) are the integral boundary layer) model. When $\beta = 0$, the set of governing equations (35) and (36) reduces to the model by Sisoev *et al.*[15] and Shkadov *et al.*,[16] but our scales are different from that of Sisoev *et al.*[15] and Shkadov *et al.*[16] When the radius $r_0 \to \infty$, the governing equations (35) and (36) reduce to the equations of a falling liquid film on a planar vertical porous wall.

A. Linear stability analysis

First, the evolution equations (35) and (36) have the following base solutions:

$$\bar{h} = 1, \quad \bar{q} = \frac{Re}{2}\phi(1), \tag{37}$$

where $\phi(1) = \phi(h)|_{h=1}$.

The linear stability of base solutions (37) is investigated by applying normal mode decomposition of the following form:

$$[h, q] = [\bar{h}, \bar{q}] + [\hat{h}, \hat{q}]e^{ikz+\lambda t}, \tag{38}$$

where $[\hat{h}, \hat{q}]$ are the amplitudes of infinitesimal disturbances.

Substituting Eq. (38) into Eqs. (35) and (36), and after linearizing, we obtain

$$\lambda\hat{q} + ik\hat{\mathscr{M}} = \frac{2r_0+1}{2}\{S[(ik)^3 + \frac{ik}{(1+r_0)^2}]\hat{h} - \frac{2\hat{q}}{\phi(1)} + \frac{Re}{\phi(1)}\Phi\hat{h}\}, \tag{39}$$

$$(1+r_0)\lambda\hat{h} + ik\hat{q} = 0, \tag{40}$$

in which

$$\Phi = 2(r_0+1)^3[\ln\frac{r_0+1}{r_0} + \frac{1}{4}] - \frac{1}{2}(r_0^3 + 7r_0^2 + 9r_0 + 3) + \frac{2\beta(r_0+1)(2r_0+1)}{r_0} \tag{41}$$

and

$$\hat{\mathscr{M}} = \frac{Re^2}{4}\mathcal{F}_1\hat{h} + \frac{4\mathscr{M}_1}{Re\phi(1)}(\hat{q} - \frac{Re}{2}\Phi\hat{h}) \tag{42}$$

with

$$\mathcal{F}_1 = 3(r_0+1)^5 \ln^2\frac{r_0+1}{r_0} - \frac{1}{2}(r_0+1)^3[3(r_0+1)^2 + (2r_0+1)(4-\frac{12\beta}{r_0}) - 4\beta r_0]\ln\frac{r_0+1}{r_0} + \frac{3(2r_0+1)^2(r_0+1)}{r_0^2}\beta^2 - \frac{1}{2r_0}(r_0+1)(2r_0+1)[2(r_0+1)^2+5(2r_0+1)]\beta + \frac{(r_0+1)(2r_0+1)(6r_0^2+22r_0+11)}{8}.$$

The dispersive relation is given by

$$\lambda^2 + B\lambda + C = 0, \tag{43}$$

where $B = \frac{4ik\mathscr{M}_1}{Re\phi(1)} + \frac{2r_0+1}{\phi(1)}$ and $C = \frac{k^2}{1+r_0}(\frac{Re^2\mathcal{F}_1}{4} - \frac{2\mathscr{M}_1\Phi}{\phi(1)}) + \frac{2r_0+1}{2(r_0+1)}\{S[k^4 - \frac{k^2}{(1+r_0)^2}] + \frac{ikRe\Phi}{\phi(1)}\}$ with $\mathscr{M}_1 = \mathscr{M}|_{h=1}$. There are two roots of Eq. (43), and are denoted as λ_1, λ_2. We assume that the real part of λ_1 is larger than that of λ_2. Solving (43), we obtain

$$\lambda_1 = \frac{-B+\sqrt{B^2-4C}}{2}, \quad \lambda_2 = \frac{-B-\sqrt{B^2-4C}}{2}. \tag{44}$$

An effective growth rate λ_r is defined by the real part of λ_1, $\lambda_r = \Re(\lambda_1)$, which describes the exponent growth of the amplitude of disturbance wave. The cut-off wave number k_c is defined for the effective growth rate $\lambda_r = 0$. When the disturbance wave number k is in the range of $(0, k_c)$, any small disturbance grows. The linear wave speed is defined by the imaginary part of eigenvalue, $c = -\frac{\Im(\lambda_1)}{k}$. Ding and Liu[29] reported in their paper that surface tension was the major cause of the interfacial instability, and the system became more unstable as the non-dimensional surface tension S increased. In the following discussion, the influence of surface tension would not be discussed and S is fixed.

The comparison of effective growth rate between the *IBL* model and the linearized Navier-Stokes equations is shown in Figure 3. The results of two methods are in good agreement in the long-wave range. Results of Ding and Liu[29] showed that, for very small Re, i.e., $Re \ll 1$, the effective growth

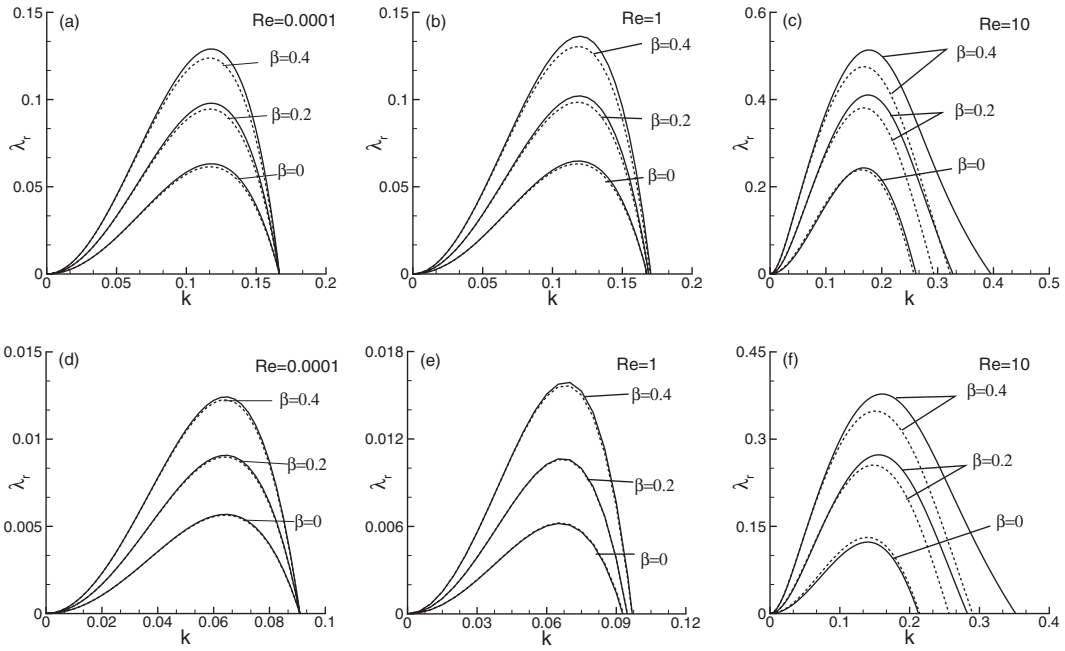

FIG. 3. The effective growth rate λ_r versus the disturbance wave number k. (a)–(c) $r_0 = 5$; (d)–(f) $r_0 = 10$. Solid lines are by the *IBL* model, and dashed lines by the linearized Navier-Stokes equations. All the figures are plotted at $S = 1000$.

rate was independent of Re, implying that the system was always unstable. Comparing Figure 3(a) with Figure 3(b) (or Figure 3(d) with Figure 3(e)), it can be observed that the growth rate changes slightly. It indicates that the interfacial instability is independent of Re when Re is very small. However, when $Re > 1$, results of the Benney-type equation[29] did not agree with the results of the linearized Navier-Stokes equations even in the long-wave range, indicating that Re should be an important factor of the dynamics of system when $Re > 1$.

When the Reynolds number $Re \geq 1$, the influence of Re on growth rate is significant as shown in Figures 3(c) and 3(f). It is observed that the larger the Re the more unstable is the system. Because the surface waves are initiated by gravity, the larger the g the more unstable is the interface. Apart from that, in Figure 3, it is shown that a larger β describes a larger growth rate of the most unstable mode. The physical mechanism is explained here. Friction in the system plays a stabilization role which decreases with increasing the value of β. Therefore, the system becomes more unstable for a larger β. Ding and Liu[29] assumed that, for a liquid film flowing down a permeable cylinder, if there was no slip at the liquid-porous interface, then the permeable cylinder should be replaced by an impermeable cylinder with a smaller radius $r \approx r_0 - \beta$. The comparison between Figures 3(a)–3(c) and Figures 3(d)–3(f) indicates that the smaller the radius the more unstable is the system. Thus, the system becomes more unstable for a larger β.

Figure 4 shows the linear wave speed c versus disturbance wavenumber k. It is observed that when Re is very small, in the long wave range, the linear wave speed c is independent of k, and the results agree with those of Klikhandler *et al.*[11] and Ding and Liu.[29] When Re approaches zero and k exceeds a certain value, a bifurcation phenomenon is observed, i.e., there are two complex conjugates c. However, the bifurcation phenomenon cannot be observed in Ding and Liu's model.[29] In the present paper, the lower branches in Figures 4(a) and 4(d) are not shown. When the Reynolds number Re is moderate, i.e., $Re \geq 1$, the bifurcation phenomenon disappears as seen in Figures 4(b) and 4(c), and 4(e) and 4(f). Figure 4 also shows that results of the *IBL* model are in good agreement with the linearized Navier-Stokes equations, and the linear wave speed is promoted by the permeability parameter β. To see the influence of r_0 on the linear wave speed c, k is fixed at 0.2,

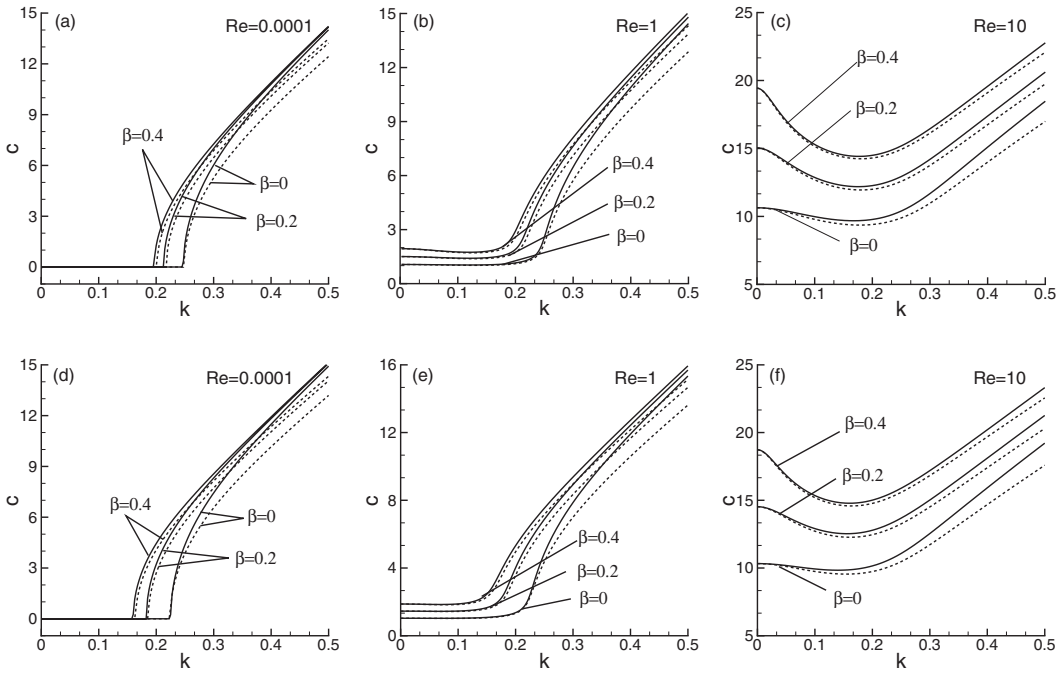

FIG. 4. The linear wave speed c versus the disturbance wave number k. (a)–(c) $r_0 = 5$; (d)–(f) $r_0 = 10$. Solid lines are by the *IBL* model, and dashed lines by the linearized Navier-Stokes equations. All the figures are plotted at $S = 1000$.

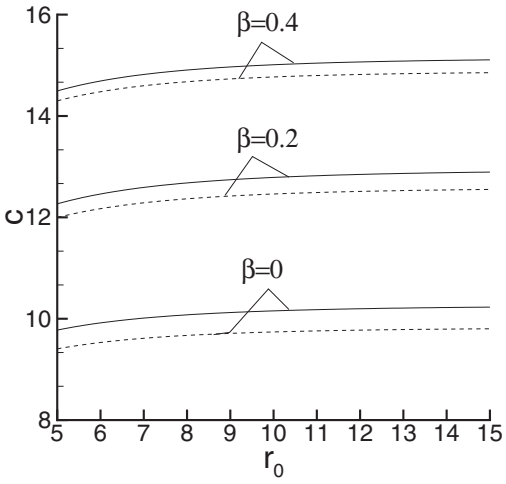

FIG. 5. The linear wave speed c versus the disturbance wave number r_0 for $Re = 10$, $k = 0.2$, and $S = 1000$. Solid lines are by the *IBL* model, and dashed lines by the linearized Navier-Stokes equations.

and $Re = 10$. The results are plotted in Figure 5. It is shown that c slightly increases with r_0, but will not change when r_0 is sufficiently large.

The marginal stability curve Re–k_c is plotted in Figure 6, which clearly shows that the system is unstable for all Re. In Figure 6, we observe that the results of the *IBL* model compare well with the linearized Navier-Stokes equation when the Reynolds number is small. In Figure 6(a) when $Re \leq 2$, and in Figure 6(b) when $Re \leq 4$, the *IBL* model agrees with the linearized Navier-Stokes equation well. The results showed that the cut-off wave number not only depends on Re, but also depends on β. It is also observed that the cut-off wave number k_c increases with increasing β, which suggests that instability of the system is enhanced by the permeability of porous medium. In the work of Ding and Liu,[29] the Benney-type model indicated that the cut-off wave number $k_c = \frac{1}{1+r_0}$ was independent of β and Re. Their results[29] did not agree with the results of linearized Navier-Stokes equations. By comparing Figure 6(a) with Figure 6(b), we observe that the liquid film is more unstable on a cylinder with a smaller radius. While the marginal stability curves of $\beta = 0$ by *IBL* agree with those obtained from the linearized Navier-Stokes equations, they start to deviate with the results of the linearized Navier-Stokes equations as the value of β increases. This suggests our model is valid for small Reynolds number when $\beta > 0$.

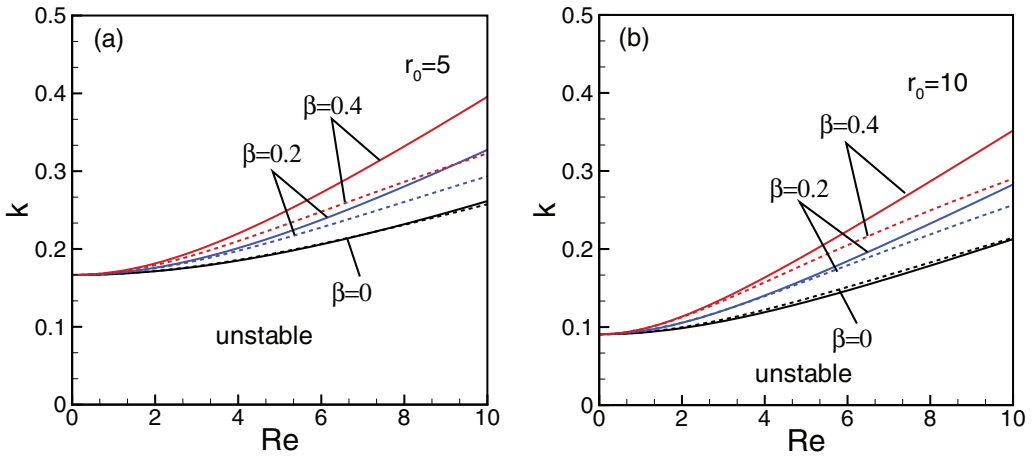

FIG. 6. Neutral stability curves in the Re–k plane when $S = 1000$. Solid lines are by the *IBL* model, and dashed lines by the linearized Navier-Stokes equations.

B. Time-dependent evolution

This section presents the evolution of the interface subjected to a finite-amplitude harmonic disturbance, so as to investigate the energy transfer from base flow to disturbance. The *IBL* model is used to examine the linear stability analysis and study the nonlinear evolution of the problem which provides the underlying nonlinear dynamics of flow system. The influence of the permeability parameter β on the nonlinear dynamics of the flow system is investigated.

At the initial time, a small harmonic disturbance is imposed on the interface, while the flow rate is not changed,

$$h(z,0) = 1 + 0.1\cos\frac{2\pi}{L}z, \quad q(z,0) = \bar{q}. \tag{45}$$

The computation domain is $z = [0, L]$. The solutions of Eqs. (35) and (36) are approximated by finite Fourier series,

$$h(z,t) = \sum_{-N/2}^{N/2} a_n e^{i\frac{2\pi}{L}nz} + c.c, \quad q(z,t) = \sum_{-N/2}^{N/2} b_n e^{i\frac{2\pi}{L}nz} + c.c. \tag{46}$$

The second-order Runger-Kutta method is applied for automatic adjustment of initial increment and for computation of the starting values. The dimensionless radius of porous cylinder is fixed at $r_0 = 5$, and the dimensionless surface tension is fixed at $S = 1000$.

We begin with the numerical study of evolution problem by setting $Re = 0.0001$ to investigate the evolution of free surface under the action of surface tension. The length of computation domain is fixed at $L = 200$. To resolve this problem, 128 Fourier modes were used. In Figure 7, the evolution of the interfacial shape is plotted for different values of β. It can be seen that, for a larger β, the evolution of interface shape is much quicker, indicating that the growth rate of disturbance is larger. This phenomenon shows that the system is more unstable for a larger β. In Figure 7(a), numerical results show that the film does not rupture for a long time. Lister *et al.*[31] pointed out that it took an infinitely long time for the film to rupture on the surface of a solid impermeable cylinder. In Figures 7(b) and 7(c), rupture phenomenon is observed. Ding and Liu[29] reported the rupture phenomenon for $\beta > 0$ in their paper. Figure 8 shows the evolution of minimum and maximum thicknesses of liquid film, indicating that the film ruptures at a faster rate for a larger β. Our results are in good agreement with those of Haimovich and Oron[30] for the non-oscillation case.

The interfacial shapes of liquid film for $Re = 1$ with different values of β are shown in Figure 9. It is observed that there is only one principal hump in each figure. At each wave front, there is a very small capillary wave. Such a wave is called "solitary wave." The results show that the larger the β the larger is the amplitude of wave. In Ding and Liu's paper,[29] such wave structures were not studied. This wave presents a sliding droplet-like shape and is of particular interest.[2] Further discussion of the droplet-like wave will be presented in Sec. IV.

We further studied the nonlinear evolution of the system by setting $Re = 10$. 256 Fourier modes are used, which provides adequate resolution of calculation. The finite-amplitude disturbance evolves

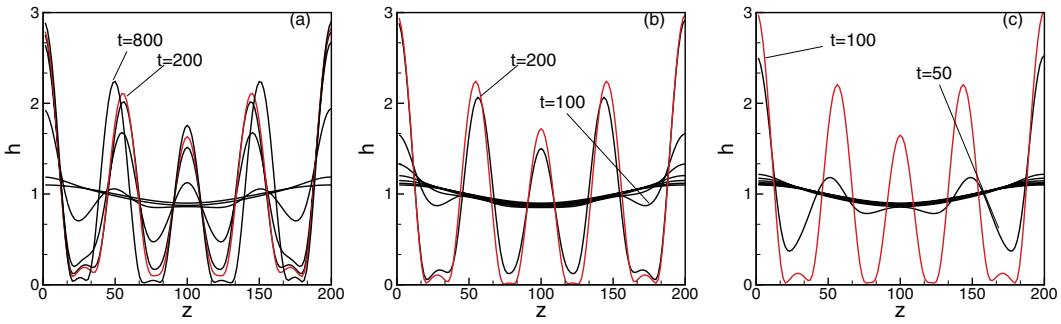

FIG. 7. Profiles of the interfacial shape for different values of β. (a) $\beta = 0$, (b) $\beta = 0.2$, and (c) $\beta = 0.4$.

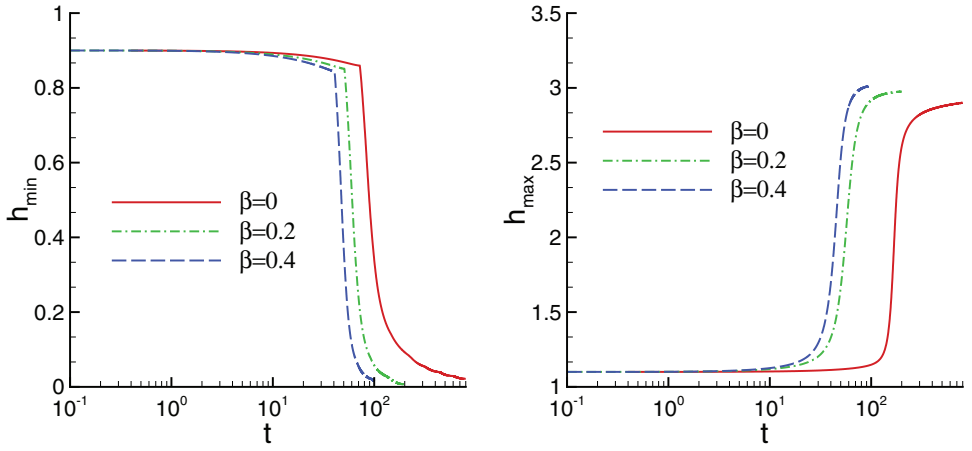

FIG. 8. The minimum and maximum thicknesses of the liquid film versus time t.

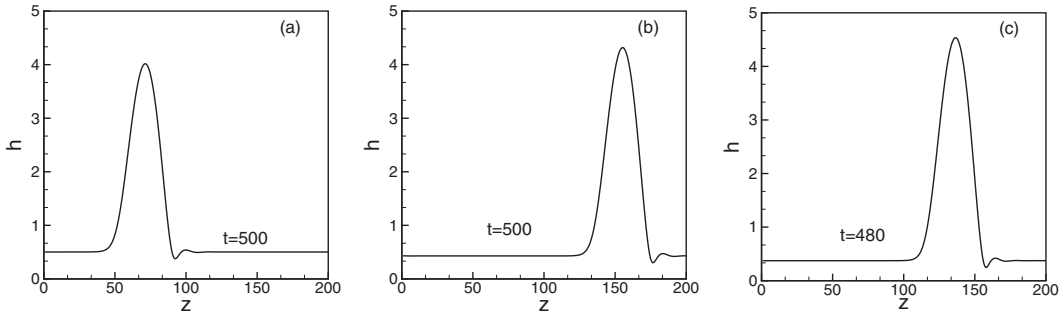

FIG. 9. Profiles of the interfacial shape for $Re = 1$. (a) $\beta = 0$, (b) $\beta = 0.1$, and (c) $\beta = 0.2$.

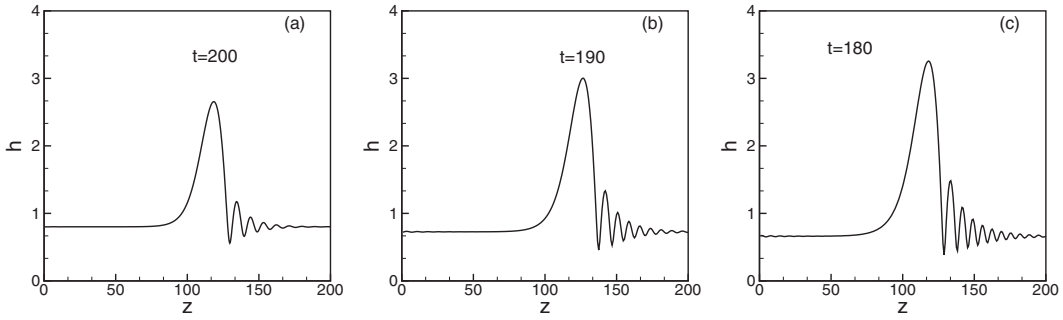

FIG. 10. Profiles of the interfacial shape for $Re = 10$. (a) $\beta = 0$, (b) $\beta = 0.1$, and (c) $\beta = 0.2$.

into a solitary wave as shown in Figure 10. The wave front oscillates much stronger than what is observed in Figure 9. The oscillation behavior at wave front is not time-dependent which can be promoted by the porous medium.[26] Figure 10 shows that the larger the β the higher is the principal hump. Ding and Liu[29] did not observe such solitary waves of the Benney-type model because their model neglected the inertia term in the streamwise momentum equation. Their model can only describe the behavior of the system at very small flow rate, which indicates that the Benney-type model[29] fails to describe strong nonlinear phenomenon.

To illustrate the solitary wave solution of this system, we apply dynamical system theory. The system of Eqs. (35) and (36) can be recast to a three dimensional dynamical system by defining a phase space spanned by $\mathbf{H} = (h, h_z, h_{zz})$. Solution of the dynamical system is homoclinic trajectory in the phase plane as seen in Figure 11. As shown in Figure 11, the finite-amplitude disturbance

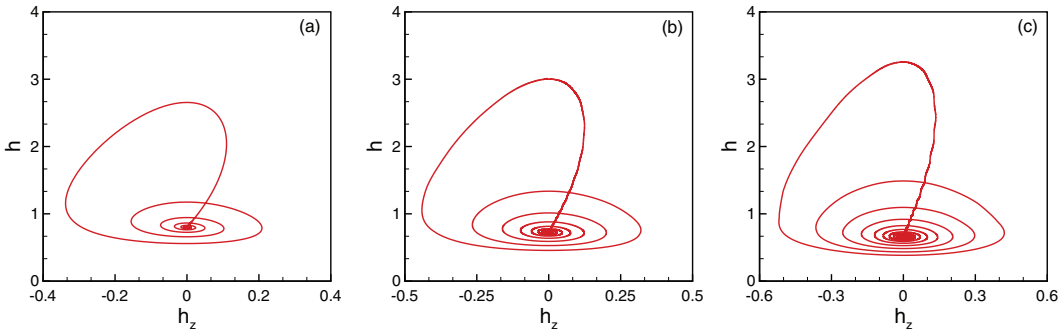

FIG. 11. Homoclinic trajectory for $Re = 10$. (a) $\beta = 0$, (b) $\beta = 0.1$, and (c) $\beta = 0.2$.

evolves into a new state. Figure 11 also indicates that the oscillation at wave front is stronger for a larger β. Actually, the oscillation at wave front is due to the nature of solitary waves. At the wave front, the thickness of the film presents damped oscillations; while at the rear of the wave, it relaxes to be constant without oscillations. Such oscillating behavior can also be promoted by increasing the Reynolds number,[32] if we compare the results in Figures 9 and 10. It was also found that for a larger β, for example, $\beta = 0.4$, the rupture phenomenon was observed. However, this phenomenon would not be discussed here.

IV. DROPLET-LIKE WAVES

This section discusses a unique phenomenon of Eqs. (35) and (36) which is shown in Figure 9. The wave travels without deformation in a moving frame relative to the stationary coordinate at a constant velocity c. The constant velocity c is studied in this section.

A. Shkadov scalings

The system is rescaled by using the Shkadov scalings as follows:

$$h^* = Hh, \quad r^* = r_0 + Hy, \quad z^* = \frac{H}{\kappa}z, \quad w^* = W_0 w, \quad u^* = \kappa W_0 u, \quad t^* = \frac{H}{\kappa W}t, \quad p^* = \rho W_0^2 p. \tag{47}$$

The variables with superscript * are dimensional parameters. H is the height of the thin film at far upstream. W_0 is the scale of velocity which refers to the mean velocity of base flow. κ is a stretching parameter, $\kappa^2 \ll 1$.

The rescaled nonlinear evolution equations are

$$q_t + M_z = \frac{1}{5\delta_\epsilon}(1 + \frac{\epsilon h}{2})\{h[h_{zzz} + (\frac{\epsilon}{\kappa(1+\epsilon h)})^2 h_z + 1] - q\frac{\varphi(1)}{h^2\varphi(h)}\}, \tag{48}$$

$$(1 + \epsilon h)h_t + q_z = 0, \tag{49}$$

where $\epsilon = H/r_0, \delta_\epsilon = 9\delta\varphi^2(\epsilon)$ with $\delta = \frac{1}{45\nu^2}(\frac{\rho g^4 H^{11}}{\sigma_0})^{1/3}$, and $\kappa = ((45\delta)^2 Ka^{-3})^{1/11}$ with $Ka = \frac{\sigma_0}{\rho(g\nu^4)^{1/3}}$. Ka is the Kapitza number. The flow rate q now is defined as $q = \int_0^h (1 + \epsilon y)w dy$. The expression $M = \int_0^h (1 + \epsilon y)w^2 dy = \frac{q^2}{16\epsilon^5 h^6 \varphi^2(h)}F$, where

$$\begin{aligned} F =& 2(1+\epsilon h)^6 \ln^2(1+\epsilon h) - (1+\epsilon h)^4[3(1+\epsilon h)^2 - 2 - 4\beta\epsilon^2 h(2+\epsilon h)]\ln(1+\epsilon h) \\ &+ 2\epsilon^5 h^3(2+\epsilon h)^3\beta^2 - \epsilon^3 h^2[3(\epsilon h+1)^2 - 1](2+\epsilon h)^2\beta \\ &+ [\frac{17}{12}(\epsilon h)^6 + \frac{17}{2}(\epsilon h)^5 + \frac{75}{4}(\epsilon h)^4 + \frac{55}{3}(\epsilon h)^3 + \frac{15}{2}(\epsilon h)^2 + \epsilon h] \end{aligned} \tag{50}$$

and

$$\varphi(h) = \frac{4(1+\epsilon h)^4 \ln(1+\epsilon h) - [(\epsilon h+1)^2 - 1][3(\epsilon h+1)^2 - 1] + 4\beta\epsilon^3 h^2(2+\epsilon h)^2}{16(\epsilon h)^3}. \quad (51)$$

When $\beta = 0$, the model reduces to the model by Sisoev *et al.*[15]

B. Non-deformation solution

The non-deformation solution of Eqs. (48) and (49) is solved by introducing the traveling wave transformation $\zeta = z - ct$. Furthermore, we set $h(z, t) = h(\zeta)$, $q(z, t) = q(\zeta)$, and denote derivatives with respect to ζ by primes. In the far upper stream $\zeta \to -\infty$ and down stream $\zeta \to +\infty$, the following boundary boundary conditions are considered:

$$h \to 1, \quad q \to 1. \quad (52)$$

Integrating Eq. (49) with the boundary conditions (52), we obtain

$$q = c[\frac{\epsilon}{2}(h^2 - 1) + h - 1] + 1. \quad (53)$$

Substituting the expression of q into the momentum equation (48), we obtain

$$h^3 h''' + G(c, h)h' + H(h, c) = 0, \quad (54)$$

where $G(c, h) = \frac{5\delta_\epsilon h^2}{1+\frac{\epsilon h}{2}}[c^2(1+\epsilon h) - M_h] + (\frac{\epsilon}{\kappa(1+\epsilon h)})^2 h^3$ and $H = h^3 - \frac{\varphi(1)}{\varphi(h)}\{c[\frac{\epsilon}{2}(h^2-1) + h - 1] + 1\}$ with $\varphi(1) = \varphi(h)|_{h=1}$ and $M_h = \frac{\partial M}{\partial h}$.

In the phase space $\mathbf{H} = (h, h', h'')$, Eq. (54) has a singular point (1, 0, 0). Let us consider the asymptotic behavior of the system near the singular point (1, 0, 0). Introducing $h = 1 + \psi$, where $\psi \ll 1$, Eq. (54) is linearized near the singular point $(h, h', h'') = (1, 0, 0)$. The linearization of term $H(h, c)$ gives

$$\hat{H} = [3 + \frac{\varphi_h(1)}{\varphi(1)} - c(1+\epsilon)]\psi, \quad (55)$$

where $\varphi_h(1) = \frac{\partial\varphi}{\partial h}|_{h=1}$. For the fast waves, it is required that

$$c > \frac{3+\varphi_1}{1+\epsilon}, \quad (56)$$

where $\varphi_1 = \frac{\varphi_h(1)}{\varphi(1)}$. When $\epsilon \to 0$ and $\beta = 0$, the wave speed $c > 3$ which agrees with that of a falling liquid film on a vertical planar surface.[33]

C. Numerical results

Let us consider $c = \frac{3+\varphi_1}{1+\epsilon} + e$ and $h = 1 + e\psi$, and substitute the expressions of c and h into Eq. (54), where e is a small positive number. After retaining the dominant term, we obtain

$$\psi''' + \bar{G}\psi' + e\psi[(3 + \frac{\epsilon(3+\varphi_1)(2\varphi_1(1+\epsilon) - \epsilon)}{2(1+\epsilon)})\psi - (1+\epsilon)] = 0, \quad (57)$$

where $\bar{G}$ is the value of $G(c, h)$ by setting $c = \frac{3+\varphi_1}{1+\epsilon}$ and $h = 1$.

Using the following transformation:

$$\zeta' = e^{1/3}\zeta, \quad (58)$$

Eq. (57) is modified as

$$\psi''' + \varsigma\psi' + \psi[(3 + \frac{\epsilon(3+\varphi_1)(2\varphi_1(1+\epsilon) - \epsilon)}{2(1+\epsilon)})\psi - (1+\epsilon)] = 0, \quad (59)$$

where $\varsigma = e^{-2/3}\bar{G}$ and is assumed to be of order $O(1)$.

Equation (59) can be recast to a three-dimensional dynamical system,

$$\psi'_1 = \psi_2, \tag{60}$$

$$\psi'_2 = \psi_3, \tag{61}$$

$$\psi'_3 = -\varsigma\psi_2 - \psi_1[(3 + \frac{\epsilon(3+\varphi_1)(2\varphi_1(1+\epsilon)-\epsilon)}{2(1+\epsilon)})\psi_1 - (1+\epsilon)]. \tag{62}$$

(0, 0, 0) is a singular point of this dynamical system. The linear behavior near this singular point is investigated. After linearizing Eq. (59) near the singular point (0, 0, 0), we obtain

$$\psi''' + \varsigma\psi' - (1+\epsilon)\psi = 0. \tag{63}$$

The characteristic equation of Eq. (63) has one real root:

$$\omega_1 = \frac{1}{6}J^{1/3} - 2aJ^{-1/3}, \tag{64}$$

where $a = \varsigma$ and $J = 108b + 12\sqrt{12a^3 + 81b^2}(b = (1+\epsilon))$. In this paper, only solitary waves are considered. Thus, ω_1 is real and positive and the other two roots are complex conjugates with negative real parts. Since $\omega_1 > 0$, the critical point (0, 0, 0) is unstable which defines a one-dimensional unstable manifold in the phase space. While the real parts of the other two roots are negative which defines a two-dimensional stable manifold in the phase space. Hence, the wave front and the wave rear are not symmetrical. At the wave front, liquid film damply oscillates to $h = 1$ as $\zeta \to +\infty$, while at the wave rear, liquid film relaxes to $h = 1$ without oscillations as $\zeta \to -\infty$.

There are two kinds of solutions of the linearized equation of Eq. (63). At the far upstream region, the solution is given by

$$\psi = C_1 e^{\omega_1 \zeta'}, \tag{65}$$

where C_1 is a small positive constant. At far downstream, solution is given by

$$\psi = C_2 e^{\omega_2 \zeta'} + C_3 e^{\omega_3 \zeta'}, \tag{66}$$

where C_2 and C_3 are small positive constants. So, the following conditions can be chosen as the initial conditions for the dynamical system (60) and (61) when $\zeta' \to -\infty$,

$$\psi_1(0) = C_1, \quad \psi_2(0) = C_1\omega_1, \quad \psi_3(0) = C_1\omega_1^2. \tag{67}$$

The dynamical system (60)–(62) is solved by the fourth-order Runge-Kutta method. C_1 is fixed at 10^{-5}. The integration is sensitive to the value of ς as mentioned by Pumir *et al.*[12] The dichotomy method was used to refine the value of ς to make $\psi \to 0$ at far downstream domain.

Equation (54) is solved by a global Fourier pseudospectral expansion:

$$h = \sum_{-N}^{N} H_k e^{i(2\pi/L)k\zeta}. \tag{68}$$

We used $N = 400$ Fourier modes to solve the problem. The Newton-Kantorovich iteration method is used to solve the nonlinear problem. The initial values of h and c for iteration are chosen as $h = 1 + e\psi$ and $c = \frac{3+\varphi_1}{1+\epsilon} + e$.

The phase velocity c is normalized to $c' = c\varphi(1)$ (Shkadov *et al.*[16]), and the results are shown in Figure 12. It can be observed that the normalized phase velocity c' increases with increasing β.

Figure 13 shows the interfacial shape and the phase orbit of a typical case. As observed, there is only one hump, in the front of which there is a very small capillary wave. In Figure 13(a), the interfacial shape of liquid film is very similar to the result in Figure 9. The numerical results show that the normalized phase velocity increases with increasing permeability of the porous cylinder indicating that the sliding effect enhances the instability of the system.

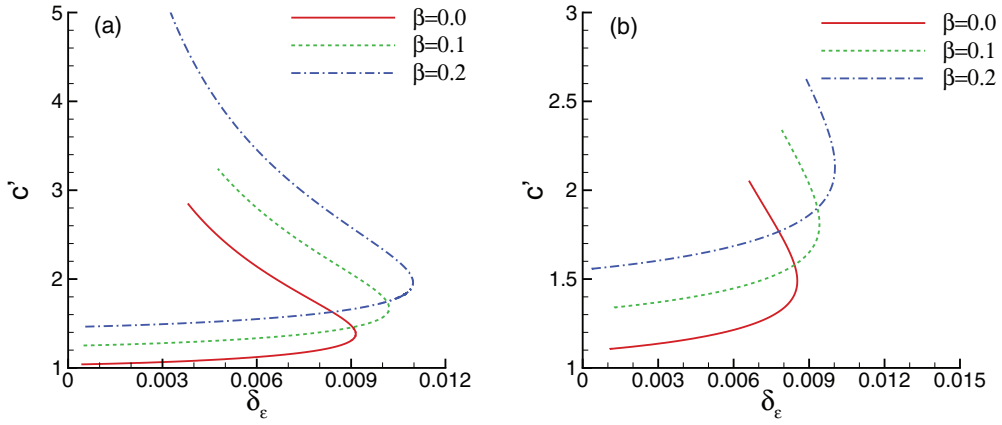

FIG. 12. Normalized phase velocity c' for the first kind solitary wave. (a) $\epsilon = 0.1$, $\kappa = 0.4$; (b) $\epsilon = 0.2$, $\kappa = 0.4$.

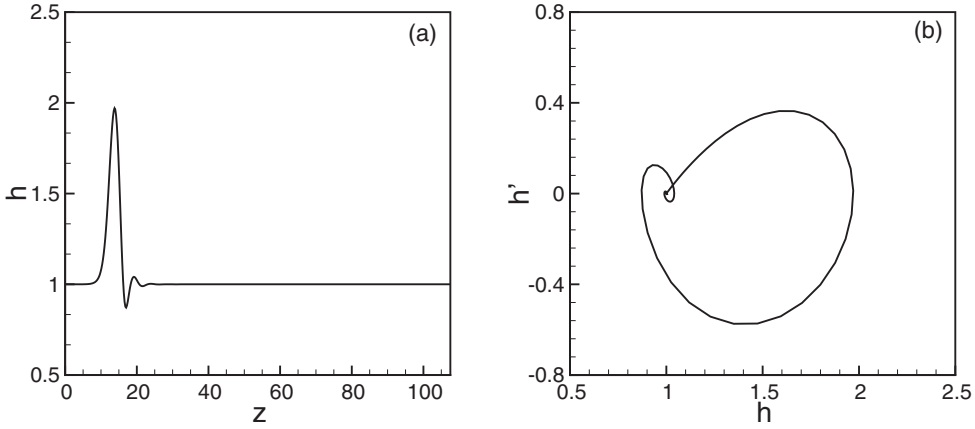

FIG. 13. (a) One representative of the solitary wave; (b) the homoclinic orbit. The other parameters are $\epsilon = 0.2$, $\beta = 0.1$, $\kappa = 0.4$, $c' = 2.338986$, $\delta_\epsilon = 0.007915$, and $Re = 0.3599$.

V. CONCLUSION

This paper investigated the stability and dynamics of a liquid film flowing down a vertical porous cylinder. Fluids in the porous cylinder were assumed to be governed by the Darcy's law. The Beavers-Joseph formula of boundary conditions at the liquid-porous interface was reduced to Navier slip condition. Two coupled equations governing the film thickness h and flow rate q based on the Prandtl boundary layer equations were derived to study the linear stability and nonlinear evolution of the flow system. Results showed that the permeability of the porous cylinder enhanced the instability of the flow system. It was observed that the cut-off wave number was increased as the permeability and Reynolds number increased. Nonlinear evolution study showed that, for very small Reynolds number Re, the rupture phenomenon was observed when permeability parameter $\beta > 0$. The rupture time decreased with increasing β. For moderate Re, the interfacial shape presented a solitary-wave structure. The oscillation behavior at the front of the solitary wave was promoted by porous substrate. The rupture phenomenon for large β was observed.

The droplet-like wave phenomena were observed when $Re = 1$ by nonlinear evolution studies. Further discussion on the droplet-like wave phenomenon in the liquid film was investigated by introducing the Shkadov scalings and traveling wave transformation. The Newton-Kantorovich method was employed to solve the reduced ordinary equation. Results showed that the nonlinear phase speed of such droplet-like wave increased with increasing β.

ACKNOWLEDGMENTS

Rong Liu gratefully acknowledges research support from National Natural Science Foundation of China (Grant No. 11102211). The authors gratefully acknowledge the referees for their many helpful comments. Ding Zijing thanks Mr. Sabnavis Bindumadhav for his suggestions.

[1] P. Kapitza and S. Kapitza, "Wave flow of thin viscous liquid films. III. Experimental study of wave regime of a flow," J. Exp. Theor. Phys. **19**, 105–120 (1949).
[2] D. Quéré, "Thin films flowing on vertical fibers," Europhys. Lett. **13**, 721–726 (1990).
[3] S. Zuccher, "Experimental investigations of the liquid-film instabilities forming on a wire under the action of a die," Int. J. Heat Fluid Flow **29**, 1586–1592 (2008).
[4] C. Duprat, C. Ruyer-Quil, and F. Giorgiutti-Dauphiné, "Experimental study of the instability of a film flowing down a vertical fiber," Eur. Phys. J. Spec. Top. **166**, 63–66 (2009).
[5] L. Rayleigh, "On the capillary phenomena of jets," Proc. R. Soc. London **29**, 71–97 (1897).
[6] J. Eggers, "Nonlinear dynamics and breakup of free-surface flows," Rev. Mod. Phys. **69**, 865–930 (1997).
[7] S. Goren, "The instability of an annular thread of liquid," J. Fluid Mech. **12**, 309–319 (1962).
[8] S. P. Lin and W. C. Liu, "Instability of film coating of wires and tubes," AIChE J. **21**, 775–782 (1975).
[9] A. De Ryck and D. Quéré, "Inertial coating of a fiber," J. Fluid Mech. **311**, 219–237 (1996).
[10] A. L. Frenkel, "Nonlinear theory of strongly undulating thin films flowing down vertical cylinders," Europhys. Lett. **18**, 583–588 (1992).
[11] I. Kliakhandler, S. Davis, and S. Bankhoff, "Viscous beads on vertical fibre," J. Fluid Mech. **429**, 381–390 (2001).
[12] A. Pumir, P. Manneville, and Y. Pomeau, "On solitary waves running down an inclined plane," J. Fluid Mech. **135**, 27–50 (1983).
[13] Yu. Ya. Trifonov, "Steady-state traveling waves on the surface of a viscous liquid film falling down on vertical wires and tubes," AIChE J. **38**, 821–834 (1992).
[14] R. Craster and O. Matar, "On viscous beads flowing down a vertical fibre," J. Fluid Mech. **553**, 85–105 (2006).
[15] G. M. Sisoev, R. V. Craster, O. K. Matar, and S. V. Gerasimov, "Film flow down a fibre at moderate flow rates," Chem. Eng. Sci. **61**, 7279–7298 (2006).
[16] V. Ya. Shkadov, A. N. Beloglazkin, and S. V. Gerasimov, "Solitary waves in a viscous liquid film flowing down a thin vertical cylinder," Mosc. Univ. Mech. Bull. **63**, 122–128 (2008).
[17] C. Ruyer-Quil and P. Manneville, "Modeling film flows down inclined planes," Eur. Phys. J. B **6**, 277–292 (1998).
[18] C. Ruyer-Quil and P. Manneville, "Improved modeling of flows down inclined planes," Eur. Phys. J. B **15**, 357–369 (2000).
[19] C. Ruyer-Quil, P. Treveleyan, F. Giorgiutti-Dauphiné, and S. Kalliadasis, "Modeling film flows down a fibre," J. Fluid Mech. **603**, 431–462 (2008).
[20] C. Ruyer-Quil and S. Kalliadasis, "Wavy regimes of film flow down a fiber," Phys. Rev. E **85**, 046302 (2012).
[21] G. Beavers and D. Joseph, "Boundary conditions at a naturally permeable wall," J. Fluid Mech. **30**, 197–207 (1967).
[22] J. Pascal, "Linear stability of fluid flow down a porous inclined plane," J. Phys. D **32**, 417–422 (1999).
[23] J. Pascal, "Instability of power-law fluid flow down a porous incline," J. Non-Newtonian Fluid Mech. **133**, 109–120 (2006).
[24] I. M. R. Sadiq and R. Usha, "Thin Newtonian film flow down a porous inclined plane: Stability analysis," Phys. Fluids **20**, 022105 (2008).
[25] B. Uma and R. Usha, "Electrified film on a porous inclined plane: Dynamics and stability," Phys. Rev. E **82**, 016305 (2010).
[26] A. Samanta, C. Ruyer-Quil, and B. Goyeau, "A falling film down a slippery inclined plane," J. Fluid Mech. **684**, 353–383 (2011).
[27] R. Liu and Q. S. Liu, "Instabilities of a liquid film flowing down an inclined porous plane," Phys. Rev. E **80**, 036316 (2009).
[28] R. Liu and Q. S. Liu, "Instabilities and transient behaviors of a liquid film flowing down a porous inclined plane," Phys. Fluids **22**, 074101 (2010).
[29] Z. J. Ding and Q. S. Liu, "Stability of liquid films on a porous vertical cylinder," Phys. Rev. E **84**, 046307 (2011).
[30] O. Haimovich and A. Oron, "Nonlinear dynamics of a thin liquid film on an axially oscillating cylinder surface," Phys. Fluids **22**, 032101 (2010).
[31] J. R. Lister, J. M. Rallison, A. A. King, L. J. Cummings, and O. E. Jensen, "Capillary drainage of an annular film: The dynamics of collars and lobes," J. Fluid Mech. **552**, 311–343 (2006).
[32] V. E. Nakoryakov, B. G. Pokusaev, and S. V. Alekseenko, "Stationary two-dimensional rolling waves on a vertical film of fluid," J. Eng. Phys. **30**, 517–521 (1976).
[33] V. Ya. Shkadov and G. M. Sisoev, "Waves induced by instability in falling films of finite thickness," Fluid Dyn. Res. **35**, 357–389 (2004).